Solidification of Binary Hypoeutectic Alloy Matrix Composite Castings

ANDREAS MORTENSEN and MERTON C. FLEMINGS

We consider a binary hypoeutectic alloy casting which solidifies in dendritic form in an unreinforced engineering casting and seek to predict its microstructure in a metal matrix composite. We focus on the case where the reinforcement is fixed in space and fairly homogeneously distributed. We assume that the reinforcement does not catalyze heterogeneous nucleation of the solid. We show that the reinforcement can cause several microstructural transitions in the matrix alloy, depending on the matrix cooling rate, the width, Λ, of interstices left between reinforcing elements, and the initial velocity V of the solidification front. These transitions comprise the following: (1) coalescence of dendrite arms before solidification is complete, causing solidification to proceed in the later stages of solidification with a nondendritic primary phase mapping the geometry of interstices delineated by reinforcement elements; (2) sharp reduction or elimination of microsegregation in the matrix by diffusion in the primary solid matrix phase; and (3) a transition from dendrite to cell formation, these cells featuring significant undercoolings or a nearly plane front configuration when reinforcing elements are sufficiently fine. Quantitative criteria are derived for these transitions, based on previous work on composite solidification, observations from directional solidification experiments, and current solidification theory. Theory is compared with experimental data for aluminum-copper alloys reinforced with alumina fibers and for the dendrite to cell transition using data from directional succinonitrile-acetone solidification experiments. Theory and experiment show good agreement in both systems.

I. INTRODUCTION

METAL matrix composite solidification processes, in which a reinforcing phase and a metal are combined while the latter is fully or partly liquid, have gained in engineering importance over the past decade, owing to their low cost, their capacity for net-shape component fabrication, and the high microstructural integrity that can be produced in the resulting material. Several different classes of composite solidification processes exist, such as infiltration or spray casting; however, an important step in all of these composite production processes is that in which the liquid metal matrix solidifies and acquires a microstructure.

It is now well known that rules developed for solidification of unreinforced metals can not be applied directly to metal matrix composites. In the matrix of a composite, the solid phase must grow within the confines of narrow interstices left between neighboring elements of the reinforcing phase, such as fibers, whiskers, or particles. The reinforcing phase thus places an upper limit on any microstructural element within the growing solid matrix while also affecting capillary equilibria, heat flow, diffusion, and fluid transport, all of which govern the progress of matrix solidification. Composite matrix microstructures can therefore be quite different from what would be expected in the same unreinforced alloy solidified under similar conditions.

ANDREAS MORTENSEN, Professor, and MERTON C. FLEMINGS, Professor, are with the Department of Materials Science and Engineering, Massachusetts Institute of Technology, Cambridge, MA 02139.

This article is based on a presentation made at the "Analysis and Modeling of Solidification" symposium as part of the 1994 Fall meeting of TMS in Rosemont, Illinois, October 2–6, 1994, under the auspices of the TMS Solidification Committee.

There has, for this reason, been considerable recent scientific interest in the solidification of metal matrix composites. Experimental and theoretical studies, which have been summarized in several reviews,[1,2,3] have thus addressed various aspects of the solidification of reinforced metals, such as dendrite tip growth conditions, solidification morphology transitions, and alterations in matrix microsegregation.

An important tool in the study of alloy solidification is the Bridgman furnace, which produces well-controlled steady-state directional solidification conditions. Steady-state directional solidification experiments consist of pulling a long sample of material at a constant speed through a region of steeply descending temperature. In the investigation of transparent metal analogue materials, this region is placed within an optical microscope for direct examination of the growing solid, while with metals, the solidifying sample is pulled rapidly into the heat sink of the apparatus to quench the solidification microstructure for subsequent metallographic characterization. These experiments, which have produced a wealth of experimental solidification data for unreinforced metals, can be extended to composites if the reinforcement surface is everywhere parallel to the temperature gradient. This approach has been used in several studies of composite solidification, reviewed in Reference 3.

Directional solidification experiments can, for a given binary alloy, be used to investigate solidification modes that span the spectrum between plane-front solidification at high thermal gradient G and low growth velocity V to cellular solidification and then to dendrite growth at the higher values of V and lower values of G. In practice, however, alloy solidification in engineering castings is generally dendritic, and solidification velocities and temperature gradients are

neither measured nor constant over the course of solidification.

We take this observation as our starting point and consider a simple binary hypoeutectic alloy cooled under conditions which lead to dendritic solidification in the unreinforced condition. We assume that the alloy is cooled at a constant rate, so that its local volumetric enthalpy decreases at a constant rate H. In the composite, this alloy must solidify within interstices left between the reinforcing elements of the composite. We seek to derive quantitative criteria for the microstructural development of the solidifying composite matrix alloy, using results from composite directional solidification studies (recently reviewed elsewhere[3]), as well as current solidification theory. We then combine the equations we derive in graphical form to draw microstructural maps which, for a given alloy, predict the changes produced by the reinforcement on the microstructure of an otherwise dendritic unreinforced matrix.

II. ASSUMPTIONS AND GOVERNING PARAMETERS

A. *Solidification Parameters*

We consider an externally cooled, initially fully liquid hypoeutectic binary alloy reinforced with a volume fraction V_f of inert second phases roughly of the same size and homogeneously distributed. We take, for simplicity, these second phases all to be of the same size and shape, *e.g.*, spherical particles or cylindrical fibers. We assume that the reinforcements are fixed in space, as is, for example, the case in the solidification of infiltrated composites. We thus ignore the effects of particle pushing, commonly found in low-volume fraction particle-reinforced alloys.

As mentioned in Section I, most engineering alloys are sufficiently enriched in solute elements that, in practical casting processes, solidification takes place at a large departure from the onset of constitutional supercooling. Generally, therefore, unreinforced hypoeutectic alloys solidify initially in the form of dendrites of the primary phase, ending with solidification of eutectic or other phases between dendrite arms. We consider in what follows this regime of solidification and therefore make the assumption that

$$G << \frac{-mVC_0\,(1 - k)}{kD} \qquad [1]$$

where G is the local temperature gradient (assumed for simplicity to be constant across the solidification front), m the liquidus slope of the alloy, V the solidification front velocity, C_0 the average composition of the alloy, k the partition ratio, and D the solute diffusion coefficient in the liquid phase.

We do not take G or V as known parameters but instead describe, when we can, solidification conditions using the local rate of change of volumetric enthalpy, H, which is a more accessible experimental parameter in practical engineering situations. We take for simplicity H to be constant, this assumption being reasonably well obeyed in many casting processes. The value of H is easily related to more usual solidification parameters, such as the total solidification time of the composite casting t_f, the total solidification time of a similar but unreinforced casting in a similar mold t_{fu}, and the cooling rate C of the composite casting:

$$H = [1 - V_f)\,L_f + c_c\,\Delta T]\,t_f^{-1} = [(1 - V_f)\,L_f + c_c\,\Delta T]\,C\Delta T^{-1} = [L_f + c_m\,\Delta T]\,t_{fu}^{-1} \qquad [2]$$

where ΔT is the total freezing temperature range (equal to $m\,(C_0 - C_E)$, where C_E is the eutectic temperature of the alloy), V_f the volume fraction of reinforcement, L_f the volumetric heat of solidification of the matrix, and c_c and c_m the volumetric heat capacity of the composite and the matrix, respectively.

We consider solidification under conditions of negligible kinetic undercooling along the primary solid/liquid interface. Everywhere along the solid/liquid matrix interface, local equilibrium then dictates $C_s^* = kC_L^*$, where C_s^* is the solid composition at the interface, C_L^* the liquid composition at the interface, and k the equilibrium partition ratio. For simplicity, we take the phase diagram to feature straight liquidus and solidus lines, such that k and the liquidus slope, m_L, are constant.

We consider, as mentioned, a casting in which the matrix of the composite is initially fully liquid and which is cooled at a rate that is typical of usual engineering situations. There are, therefore, no internal heat sources or sinks within the composite, as when an initially cold preform is infiltrated with liquid metal: in such a case, the metal is rapidly chilled by the reinforcement as it comes into contact with the latter and solidifies partially *via* rapid removal from the matrix by the fibers.[4,5] This novel solidification mode, special to infiltrated composites, is not considered here.

The time for temperature equilibration within the reinforcement (usually the phase of lesser thermal conductivity in the composite) is on the order of d^2/α, where d is the smaller transverse dimension of the reinforcement (the diameter of fibers or spheres, the thickness of plates, *etc.*) and α its thermal diffusivity. Since $d \leq 100$ μm in most metal matrix composites, and since α is seldom much lower than 10^{-6} m^2 s^{-1}, this time is at most on the order of 10 milliseconds, generally less. It is, therefore, only in rapid solidification processes, featuring solidification times far below 1 second (such as those modeled in Reference 6), or with very large reinforcements (such as the fibers of diameter on the order of a centimeter modeled in[7,8]), that thermal effects need be considered.

We consider here castings typical of engineering materials and solidification processes, having reinforcements no larger than 100 μm and local solidification times greater than about 1 second; hence, matrix and fiber have ample time to equilibrate their temperature on a local scale. Because of the high rate of local temperature equalization between matrix and reinforcement, and because the rate of alloy solidification is governed by solute diffusion, it can therefore safely be assumed that during solidification, matrix and fiber temperatures are equal and uniform locally within the composite. The only significant temperature gradients in the composite casting are thus on the scale of the casting and are described by macroscopic heat transport equations applied across the composite casting treated as a continuum.

B. *Capillarity*

Capillary forces are well known to exert a considerable influence on the solidification of metals. In composites,

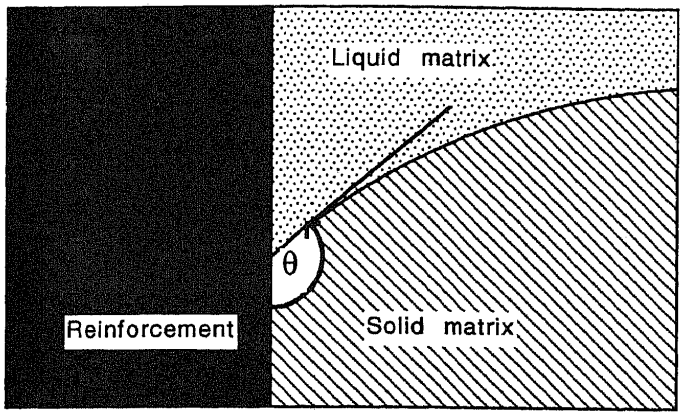

Fig. 1—Definition of the contact angle θ of the solid metal on the reinforcement in the presence of the liquid.

these take on added importance because of the presence of capillary equilibria along the contact line between the liquid/solid matrix interface and the matrix/reinforcement interface. Since the reinforcement is generally a nondeforming solid at matrix solidification temperatures, equilibrium along this contact line introduces one new parameter in the solidification of composites, namely, the contact angle θ of the primary solid metal on the reinforcement in the presence of the liquid metal, defined in Figure 1. This angle is the same as that which is considered in elementary treatment of the thermodynamics of heterogeneous nucleation. In composites, θ is thus important both in the nucleation and in the growth of the primary solid phase. If θ is small, the matrix tends to nucleate on the reinforcement and to grow along the matrix/reinforcement interface, an effect which was illustrated in directional solidification experiments with transparent metal analogues.[9,10,11]

Generally, capillary forces do not favor contact of the solid phase with the reinforcement surface, meaning that θ is large in most composite systems. The solid phase then nucleates and grows away from the reinforcement in most engineering composites. This is apparent in the fact that in most composite systems, the reinforcement is not an efficient site for catalysis of matrix solidification,[2] resulting in large matrix grains, which are seldom affected by the reinforcement when the composite is cooled slowly from the fully liquid matrix state. This was further confirmed microscopically in directional solidification experiments for Al-Cu alloys reinforced with aluminum oxide fibers.[12,13] Known exceptions to this rule are hypereutectic Al-Si alloys reinforced with graphite, SiC, SiO_2, and Al_2O_3,[2,14] Al-4.5 wt pct Cu reinforced with TiC,[15] Ti-51.5Al-1.4Mn reinforced with TiB_2 particles,[16] and magnesium alloy AZ91 reinforced with SiC particles.[17]

We assume in what follows that θ is large, *i.e.*, that capillary forces favor contact of the liquid with the reinforcement over contact of the solid, thus encouraging the solid to nucleate and grow at locations other than the reinforcement/matrix interface.

III. MICROSTRUCTURAL LENGTH SCALES IN COMPOSITE SOLIDIFICATION

As described in Section II, if the casting we consider were made of the unreinforced alloy, solidification would be dendritic and the first moments of growth would consist of motion of dendrite tips through untransformed liquid. The radius R of dendrite tips obeys, in unreinforced alloys, the relationship[18]

$$R = \sqrt{\frac{\Gamma}{\sigma^* \left(\frac{-m\,(1-k)\,C_t V}{D} - G \right)}} \qquad [3]$$

where C_t is the liquid composition at the dendrite tip, D the solute diffusion constant in the liquid, Γ the Gibbs–Thomson coefficient, and σ^* a constant approximately equal to 0.025. The term C_t is in the range of solidification rates found in casting processes, nearly equal to the average alloy composition, C_0. Taking $C_t \approx C_0$ and with account of assumption [1], this expression can be simplified to become

$$R = \sqrt{\frac{-D\Gamma}{\sigma^* m\,(1-k)\,C_0 V}} \qquad [4]$$

This quantity sets the first microstructural dimensional scale of the growing solid phase. As solidification progresses, secondary arms form, grow, and coarsen. The initial microstructural scale R in the matrix is then erased to become the spacing of dendrite arms, λ, which sets the scale of matrix microstructural features and obeys the well-known law whereby λ is proportional to the cubic root of solidification time:[19]

$$\lambda = Kt^{1/3} \qquad [5]$$

where K is a constant.

In the composite casting we consider, the matrix must solidify within the narrow interstices left between the various elements of the reinforcing phase. This places a restriction on allowable dimensions of microstructural elements that evolve in the solidifying matrix. The geometry of these interstices is complex; however, at the simplest level of analysis, we seek to characterize its influence on matrix solidification *via* a single parameter, the mean free distance between reinforcement elements, Λ, defined as the average length traveled along a randomly oriented line through the matrix between reinforcing elements (fibers, particles, or other). This, in turn, equals $\overline{L_3}\,(1 - V_f)\,V_f^{-1}$, where $\overline{L_3}$ is the mean intercept length, defined as the average value of the distance traveled through each reinforcing element (fiber, particle, or other) along randomly oriented lines.[20]

Knowing $\overline{L_3}$ then allows estimation of Λ when the growth direction of matrix dendrite arms is random. For simple reinforcement shapes, $\overline{L_3}$ is given in Tables 4.1 and 4.2 of Reference 20: for a spherical reinforcement of uniform radius r, $\overline{L_3} = 4r/3$; for short fibers of uniform radius r and length h, $\overline{L_3} = 2rh\,(r + h)^{-1}$; and for long fibers of radius r, $\overline{L_3} = 2r$; *etc.* Resulting expressions for Λ are given in Table I for randomly oriented dendrites.

There are cases where matrix dendrites and reinforcement elements bear a nonrandom orientation relationship with one another: the simplest and most thoroughly investigated case is that found in directional solidification experiments, where a composite reinforced with parallel fibers is solidified such that fiber axes lie parallel to primary dendrite arms or cells. In this configuration, a better estimate of Λ is the mean free distance between fibers within the

plane perpendicular to both the fiber axes and the primary matrix growth direction. Since area fractions and volume fractions are equal, within this plane, we still have $\Lambda = \overline{L_2}\,(1 - V_f)\,V_f^{-1}$, where $\overline{L_2}$ is the mean intercept length of randomly oriented lines in a plane perpendicular with the fiber axis, simply calculated to be $\overline{L_2} = \pi r/2$.

IV. COARSENING IN REINFORCED ALLOYS

Let us assume for now that R (Eq. [3]) is much smaller than Λ. When this is the case, interference of the reinforcement with progress of the dendrite tips occurs only in the occasional event where a dendrite tip grows toward the reinforcement, approaching its surface within roughly one tip radius R, since this distance roughly equals the width of the solute-enriched region surrounding the dendrite tip. In these occasional events, as was shown experimentally in directional experiments using transparent metal analogues,[1,21–23] growth of the tip slows or stops because the reinforcement inhibits solute diffusion, and the dendrite is deflected, for example, *via* a change in leading dendrite tip to the tip of a secondary or higher order arm pointed away from the reinforcement surface. Other than these occasional encounters, when $R << \Lambda$, the dendrite tips grow in the composite essentially as they would in an unreinforced alloy, because most of the time the reinforcement does not interfere with solute evacuation from dendrite tips.

Thus, when $R << \Lambda$, the first moments of solidification lead to the formation of a network of dendrite arms similar in shape and number to those found in the unreinforced condition, save for some distortion of this structure within a distance of about R along the matrix/reinforcement interface. Therefore, as in conventional castings, the microstructure of the fully solidified alloy is predominantly determined by subsequent coarsening of this starting microstructure.

The rate of dendrite arm coarsening is limited by the rate of diffusion of solute through the liquid phase to regions of highly positive curvature (measured through the solid) from regions of lower or negative curvature (the solid phase correspondingly melts back in regions of positive curvature and grows in regions of low or negative curvature). It is known from microstructural studies of dendrite arm coarsening that this coarsening process can essentially take two forms, depending on whether highly curved solid regions melt back to deposit onto regions of positive or negative curvature. Using terminology of previous articles,[24,25] the former process is termed *ripening* and causes larger dendrite arms to grow at the expense of smaller arms, while the latter process is termed *coalescence* and causes the dendrite arms to fuse together at points of contact such as their point of common attachment of a lower order arm. Ripening causes smaller dendrite arms to disappear and, hence, the average dendrite arm spacing to increase according to Eq. [5]. Coalescence also increases the dendrite arm spacing in time but ultimately leads to a loss of the dendritic character of the solidifying matrix microstructure when most dendrite arms have fully fused together. Ripening is dominant at the beginning of solidification, when the volume fraction solid is low and dendrite arms are long and thin. Coalescence dominates at higher values of the volume fraction solid or after prolonged isothermal hold of a mushy alloy.

Table I. Mean Reinforcement Intercept Length L Giving λ as $\lambda = L\,(1\text{-}V_f)\,V_f^{1}$ for Randomly Oriented Dendrites

Reinforcement shape	L
Sphere, radius r	$4r/3$
Disk, radius r, thickness $t << r$	$2t$
Cylinder, radius r, height $h \approx r$	$\dfrac{2rh}{r + h}$
Rod, radius r (height $h >> r$)	$2r$
Cube, edge a	$2a/3$
Rectangle parallelipiped, edges a, b, and c	$\dfrac{2abc}{ab + bc + ca}$
Octahedron, edge a	$0.545a$
Hexagonal prism, edge a, height c	$\dfrac{2\sqrt{3ac}}{\sqrt{3}a + 2c}$
Tetrahedron, edge a	$0.2725a$

If we consider the semisolid dendritic matrix of a composite, it is clear that the reinforcement will interfere with ripening; when the dendrite arms thicken to approach Λ, solute diffusion from one arm to the next takes place along a path which is altered by the presence of the inert reinforcements. Even past this point, however, one can envision ripening progressing in the matrix somewhat further by diffusion of solute from one interstice to another. This last mechanism was identified experimentally in experiments on equiaxed dendritic solidification of Al-4.5 wt pct Cu reinforced with parallel alumina fibers[26] and shown experimentally to cause an increase in the time exponent of the coarsening law, from the usual value of 1/3 to 1/2. The explanation for this change in coarsening law constant lies in the fact that when ripening takes place across interstices, the diffusion distance for solute which migrates from growing to shrinking arms remains relatively constant. Therefore, if λ is the average dendrite arm spacing, solute concentration gradients which drive ripening across interstices vary in time only because curvature differences, roughly proportional to λ^{-1}, decrease in time, whereas in unreinforced alloys, these gradients vary as λ^{-2}, because diffusion distances increase proportionally with λ, while concentration differences still vary roughly as λ^{-1}. Because the rate of solid/liquid interface movement, and hence the rate of change of dendrite arm spacing $d\lambda/dt$, is proportional to concentration gradients, λ can become roughly proportional to $t^{1/2}$ when λ reaches and slightly exceeds Λ.

Dendrite arm coalescence is very strongly influenced by the reinforcement, because the length of dendrite arms is limited in the composites: dendrite arms, which are generally much longer than they are thick in unreinforced castings, cannot, in the composite, be on average much longer than $\Lambda/2$. For this reason, it takes a much shorter time for the space between dendrite arms to fill up with solid and sinter dendrite arms together in composites than in unreinforced alloys. As a consequence, the dendritic character of the matrix is much more rapidly lost in metal matrix composites.

This phenomenon was identified and analyzed for direc-

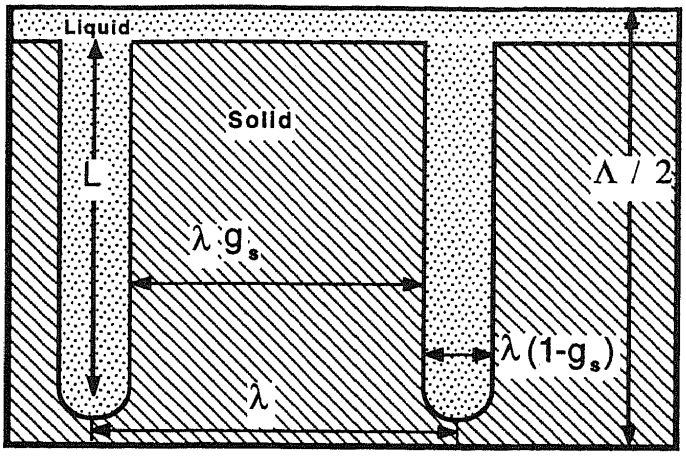

Fig. 2—Schematic description of a coalescing dendrite arm, with definition of relevant distances.

tional dendritic solidification of a parallel fiber composite in Reference 27 and can be quantified along similar lines for the general case of randomly oriented dendrite arms coalescing in interstices of average width Λ.

Consider two randomly oriented neighboring dendrite arms in an interstice. On average, their length cannot exceed Λ/2. If at time t the volume fraction of the solid phase within the metal is g_s and the average dendrite arm spacing is λ, the average width of the pool of liquid left between dendrite arms is roughly $\lambda (1 - g_s)$ (neglecting liquid between the dendrite and the fiber, the primary dendrite stem, *etc.*) (Figure 2). If we neglect interference of the reinforcement with the kinetics of ripening, λ can be estimated as being the same as in the unreinforced alloy.

If we assume that the fraction solid is given by the Scheil equation, derived for dendritic solidification with interfacial equilibrium and no solid-state diffusion, neglecting density variations with solute content and matrix solidification, we can write

$$1 - g_s = \left(\frac{C_L}{C_0}\right)^{\frac{1}{k-1}} \qquad [6]$$

where C_L is the liquid composition and C_0 the average composition of the matrix alloy. The interdendritic liquid composition C_L^κ at an interface of curvature κ is given by the Thomson–Freundlich equation:

$$C_L^\kappa = C_L + \frac{\kappa\Gamma}{m} \qquad [7]$$

where C_L is the equilibrium composition in the liquid for a flat interface and m the liquidus slope. The term Γ is the Gibbs–Thomson constant and equals the liquid-solid surface energy σ_{LS} divided by the volumetric entropy of fusion of the alloy primary constituent. We now simplify the solute concentration profile by assuming that the rate of coalescence is limited by diffusion of solute from the trough separating two dendrite arms to the arm tips, of (positive) curvature much smaller than the (negative) curvature at the bottom of the trough. Thus, we estimate the flux of solute diffusing from the trough bottom as roughly equal to

$$J = D_L \frac{C_t - C_L}{L} = D_L \frac{\kappa_t \Gamma}{L m_L} \qquad [8]$$

where C_t is the composition at the bottom of the trough, L the distance separating the dendrite arm tips from the dendrite arm trough, and κ_t the curvature at the bottom of the trough. Assuming that the bottom of the trough separating two dendrite arms is most sharply curved within the plane of the arms, κ_t can be estimated as

$$\kappa_t = \frac{-2}{\lambda (1 - g_s)} \qquad [9]$$

Now the rate dL/dt at which the dendrite arms shorten is given by the rate at which solid deposits at the bottom of the trough separating dendrite arms. This latter rate of solidification is simply given by the standard flux condition:

$$J = C_t (1 - k) \frac{dL}{dt} \qquad [10]$$

where J is the solute flux into the liquid from the solid/liquid interface at the bottom of the trough between dendrite arms. Noting that the increase in λ with time does not affect the validity of this flux balance at the bottom of the trough between surviving dendrite arms, and noting also that $C_t \approx C_L$, inserting Eqs. [5], [6], [8], and [9] into Eq. [10] yields

$$\frac{L dL}{dt} = \frac{2\Gamma D_L}{(1 - k)\, mK} \frac{1}{t^{1/3}\, C_0\, (1 - g_s)^k} \qquad [11]$$

If the rate of heat extraction H from the composite during solidification is constant,

$$(1 - V_f)\, L_f g_s - c_c m\, (C_L - C_0) = Ht \qquad [12]$$

then by inserting Eq. [6], it becomes

$$(1 - V_f)\, L_f g_s - c_c m C_0\, [(1 - g_s)^{k-1} - 1] = Ht \qquad [13]$$

so that

$$dt/dg_s = (1 - V_f)\, L_f H^{-1} - c_c m C_0 H^{-1} \qquad [14]$$
$$(1 - k)\, (1 - g_s)^{k-2}$$

Finally, D_L varies with temperature and, hence, with g_s as

$$D_L = D_0 e^{-\frac{Q}{k\,[T_m + mC_0\,(1 - g_s)^{k-1}]}} \qquad [15]$$

After insertion of Eqs. [13] through [15] into Eq. [11] one obtains

$$L dL = \frac{2\Gamma D_0}{(1 - k)\, mKC_0 H^{2/3}} \frac{[(1 - V_f)\, L_f - mc_c C_0\, (1 - k)\, (1 - g_s)^{k-2}]\, e^{-\frac{Q}{k\,[T_m + mC_0\,(1 - g_s)^{k-1}]}}\, dg_s}{\left[(1 - V_f)\, L_f g_s - mc_c C_0 \left((1 - g_s)^{k-1} - 1\right)\right]^{1/3} (1 - g_s)^k} \qquad [16]$$

The fraction solid at which dendrite arms of initial length Λ/2 are erased can then be calculated from

$$\Lambda^2 = \frac{4\Gamma D_0}{(1-k)\, mKC_0H^{2/3}} \int_0^{g_s} \frac{\left[(1-V_f)\, L_f - mc_cC_0\,(1-k)\,(1-g)^{k-2}\right] e^{-\frac{Q}{k\,[T_m + mC_0\,(1-g)^{k-1}]}}\, dg}{\left[(1-V_f)\, L_f\, g - mc_cC_0\left((1-g)^{k-1} - 1\right)\right]^{1/3} (1-g)^k} \quad [17]$$

If the fraction solid corresponding to satisfaction of Eq. [17] is higher than the fraction solid at the eutectic temperature of the alloy, gs_E, the solidified matrix microstructure will be dendritic throughout solidification. If, on the other hand, the corresponding g_s is significantly lower than g_{sE}, all dendrite arms in the matrix of the composite will have coalesced long before completion of solidification. Then, the matrix solidifies in later stages essentially as a nondendritic cellular matrix, made of islands of primary phase more or less centered between reinforcing elements. Remaining liquid matrix, and hence solute-rich primary phase and the eutectic in the fully solidified composite, are then concentrated along the reinforcement/matrix interface. The criterion for loss of dendritic character by coalescence of dendrite arms before the end of solidification is, thus,

$$H^{2/3}\,\Lambda^2 \le \frac{4\Gamma D_0}{(1-k)\, mKC_0} \int_0^{g_{sE}} \frac{[(1-V_f)\, L_f - mc_cC_0\,(1-k)\,(1-g)^{k-2}]\, e^{-\frac{Q}{k\,[T_m + mC_0\,((1-g)^{k-1}]}}\, dg}{[(1-V_f)\, L_f g - mc_cC_0\,((1-g)^{k-1} - 1)]^{1/3}\,(1-g)^k} \quad [18]$$

Equation [18] can be integrated numerically for a given system; however, considerable algebraic simplification can be achieved by making two relatively simple assumptions:

(1) we assume that D_L is approximately constant during solidification; and
(2) we take λ to be roughly constant as well.

Equation [18] then becomes

$$\Lambda^2 = \frac{4\Gamma D_L}{(1-k)\, m\lambda C_0H} \int_0^{g_s} \frac{[(1-V_f)\, L_f - mc_cC_0\,(1-k)\,(1-g)^{k-2}]\, dg}{(1-g)^k} \quad [19]$$

which is easily integrated to yield

$$\lambda H\Lambda^2 = \frac{4\Gamma D_L}{(1-k)\, mC_0} \left[(1-V_f)\, L_f \frac{[1-(1-g_s)^{1-k}]}{1-k} - mc_cC_0\,(1-k)\,[(1-g_s)^{-1} - 1]\right] \quad [20]$$

The left-hand side of Eq. [20] contains parameters which depend on the solidification conditions and on the reinforcement morphology. The right-hand side of this equation contains terms which are system parameters characteristic of the matrix alloy and the fraction solid g_s at which dendrite arms are predicted to have coalesced or, in other words, at which the microstructure has lost its initial dendritic character. A reasonable (because of the rapidly decreasing rate of dendrite arm ripening with time) and conservative estimate of λ is to take λ equal to its upper bound, namely, the dendrite arm spacing reached in the unreinforced alloy for the same solidification time. This is obtained by combining Eqs. [5], [6], and [12]:

$$\lambda = KH^{-1/3}\left[(1-V_f)\, L_f\left[1 - \left(\frac{C_E}{C_0}\right)^{\frac{1}{k-1}}\right] - mc_c\,(1-k)\,[C_E - C_0]\right]^{1/3} \quad [21]$$

The matrix thus loses its dendritic character during solidification provided

$$H^{2/3}\,\Lambda^2 \le \frac{-4\Gamma D_L}{(1-k)\, mC_0\, K}. \quad [22]$$

$$\frac{\left[(1-V_f)\, L_f \frac{C_E - C_0}{C_E\,(1-k)} - mc_cC_0\,(1-k)\left[\left(\frac{C_E}{C_0}\right)^{\frac{1}{1-k}} - 1\right]\right]}{\left[(1-V_f)\, L_f\left[1 - \left(\frac{C_E}{C_0}\right)^{\frac{1}{k-1}}\right] - mc_c\,(1-k)\,[C_E - C_0]\right]^{1/3}}$$

This expression differs somewhat from that derived in Reference 27 for the case of solidification within a tube at steady velocity in a constant temperature gradient. Differences arise from the fact that we have allowed ripening to proceed uninhibited during coalescence (whereas in the previous case λ could not exceed the tube diameter) and, from the constant rate of heat removal assumed here, a more realistic assumption for practical solidification processes.

In summary, Eq. [22] provides a relatively simple and conservative criterion for the elimination of dendrite arms by coalescence during initially dendritic solidification of the matrix in a composite. The critical quantity is seen to be $H\Lambda^3$, which is intuitively satisfying since the governing process is diffusion-limited coarsening. If the inequality in Eq. [22] is obeyed, the liquid composition at which coalescence erases the dendrite arms in the matrix can be estimated by solving Eq. [22] written as an equality for $C_L = C_E$. This composition, multiplied by k, then gives the composition of the last isoconcentrate in the solid to have a dendritic character after metallographic etching to reveal matrix coring patterns.

V. GEOMETRICAL CONSTRAINT OF DENDRITE TIP SOLIDIFICATION

We now consider the case where the radius R of a dendrite tip in the unreinforced alloy is commensurate with the interstice width, Λ. It is found in experiments on succinonitrile-acetone[9,11] and from finite-difference modeling of di-

rectional solidification[28,29]* that when Λ decreases below the primary dendrite arm spacing, all else being constant, there can be a transition from dendritic to cellular solidification. This provides a second mechanism by which dendrites may not be observed in a metal matrix composite under solidification conditions which lead to dendritic solidification in an identically processed unreinforced casting of the matrix alloy.

*We use these calculations here as a guide and without questioning the origin of the dendritic tip solutions having the proper value of σ^* that are found despite the lack of surface tension anisotropy among the assumptions made in these calculations.

It is apparent from the calculations of Lu and Hunt (Figure 1 of Reference 28 and Figures 2 and 7 of Reference 29) that the transition from dendritic to cellular solidification at falling Λ is relatively abrupt and well defined and that, following this transition, the undercooling of the corresponding cell tips reaches its minimum very close to the transition conditions. Furthermore, it is also suggested from Lu and Hunt's calculations (Figure 7 of Reference 29) and by Fabietti and Sekhar's experimental data (Figure 3) that as the tip changes from dendritic to cellular with decreasing Λ, (1) the decrease in tip radius R is small for dendrites, such that σ^* does not fall far below 0.0025, and (2) the radius is continuous across the transition from dendrite to cell. At this transition, therefore, the dendrite tip radius is not far from that given by Eq. [3] or [4] with $\sigma^* \approx 0.025$.

These observations suggest a very simple approximate criterion for the transition from dendritic to cellular solidification at falling Λ. At minimal undercooling, cell tips grow with a width of about one-half the cell spacing, or interstice width Λ, in a composite (this is rigorously true at small Peclet numbers $\Lambda V/D_L$ in two-dimensional planar interstices, these being defined as the space between two planes Λ apart).[30] Furthermore, at low Peclet numbers, dendrite tips are surrounded with a solute-enriched zone extending roughly one dendrite tip radius away from the tip surface. Provided growth does not take place at high Peclet numbers, as assumed, we may therefore infer that at the dendrite to cell transition, the tip radius roughly equals $\Lambda/4$, in fairly good agreement with the experimental data of Fabietti and Sekhar (Figure 3). Hence, the transition from dendrite tip to cell tip formation takes place under conditions where the dendrite tip R predicted by Eq. [3] reaches a maximum value of about $\Lambda/4$, *i.e.*, when

$$\Lambda^2 = \frac{16\,\Gamma}{\sigma^* \left(\frac{-m\,(1-k)\,C_t V}{D} - G \right)} \qquad [23]$$

from Eq. [3]; or since we have focused the present discussion on the case in which the unreinforced alloy G can be neglected and $C_t \approx C_0$, Eq. [4] applies and Eq. [23] can be simplified to become

$$V\Lambda^2 = \frac{-640 D\Gamma}{m\,(1-k)\,C_0} \qquad [24]$$

Except at high growth velocities (at which the dendrite tip undercooling is sufficiently large to cause C_t to exceed C_0 significantly), this latter criterion compares very well with predictions of Lu and Hunt: the locus of growth conditions over which the computed finite-difference solid tip solution passes from dendritic to cellular is predicted by Eq. [24] within a factor 2 in V (Figure 1 of Reference 28 and Figure 2 of Reference 29). Comparison with experimental data for succinonitrile-acetone is very good for growth in cylindrical interstices: for 1 wt pct acetone, the transition is predicted to occur near $V = 2$ μm/s, in good agreement with the data in Figure 3; and for 0.3 wt pct acetone, the predicted line lies within the transition regime separating dendritic and cellular growth regimes (Figure 4(a)). For succinonitrile-0.5 wt pct acetone grown in rectangular interstices, the agreement is somewhat inferior (Figure 4(b)) but still within a factor 2 in V.

In conclusion, Eq. [24] provides a simple criterion for transition from dendritic to cellular growth caused by geometrical constraint by the reinforcement in conditions where dendrites form in the unreinforced alloy, which agrees with current theoretical predictions and experimental data within a factor 2 in V.

Prediction of this transition necessitates knowledge of V, which is not uniquely known for given H. For directional solidification, full thermal analysis or extensive measurement is required to predict the rate of motion V of the isotherm corresponding to the liquidus temperature of the solidifying alloy. In equiaxed growth into an undercooled melt, V can roughly be estimated by neglecting tortuosity in the interstices, since dendrite tips will then travel a distance roughly equal to one-half the average matrix grain size d. Noting that initially most solidification takes place near the liquidus temperature (this is apparent from inspection of the Scheil equation, Eq. [6]), and knowing that at the dendrite to cell transition about half the matrix solidifies upon passage of the tip, at this transition, V is roughly equal to

$$V \approx \frac{d}{2} \frac{2H}{L_f (1 - V_f)} = \frac{dH}{L_f (1 - V_f)} \qquad [25]$$

VI. MICROSEGREGATION IN METAL MATRIX COMPOSITES

Except for interstitial solute elements, diffusion in solidifying alloys is generally too slow to erase concentration gradients in the primary phase, regardless of how slow solidification may be. The underlying explanation for this fact is that although increasing the total solidification time may decrease microsegregation somewhat (by partial solid-state diffusion and by dendrite arm ripening), at long solidification times, the average dendrite arm spacing (and hence diffusion distances) increases at too high a rate for diffusion to "keep up" and produce compositional homogenenization of the solid phase.

In a metal matrix composite, this rule is no longer obeyed: the reinforcing phase now places an upper limit on diffusion distances, since the matrix can only coarsen to the point where a nondendritic primary phase mapping the matrix/reinforcement interface is formed. Beyond this point, provided there are no great irregularities in the interstice geometry within the composite, coarsening stops. For this reason, in a composite, under conditions of slow cooling, microsegregation is significantly reduced or eliminated.

This effect was proven experimentally in directionally solidified fiber-reinforced aluminum-copper alloys, grown

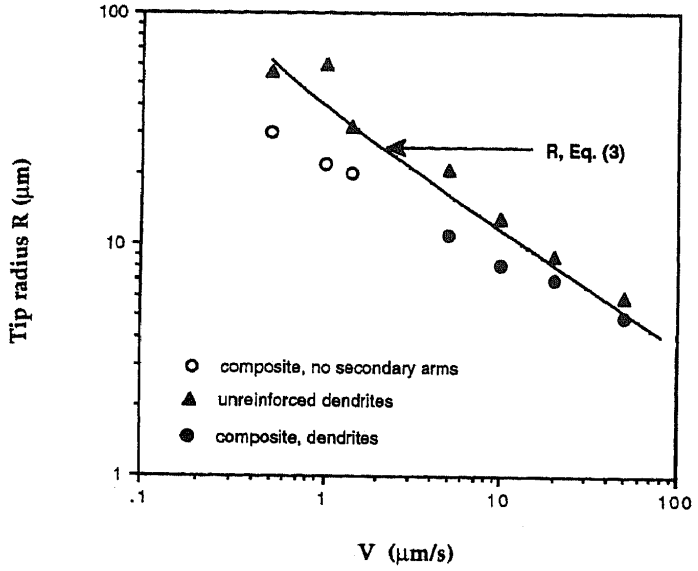

Fig. 3—Experimental measurements of dendrite and cell tip radii for succinonitrile - 1 wt pct acetone solidified directionally at steady state with $G = 3000$ K m^{-1}.[9] Data comprise tip radii for unrestricted growth between microscope slides and for growth within a cylindrical capillary of inside diameter 100 μm.

both in the cellular and the dendritic regimes.[12,27] At sufficiently low cooling rates, significant reductions in microsegregation were observed, and at the slowest cooling conditions explored, a featureless matrix free of microsegregation was formed. Theoretical analysis[27,31] showed that these observations are explained as resulting from solid-state diffusion erasing concentration gradients over distance Λ. The method used, namely, finite difference analysis of solidification in an interstice with cylindrical symmetry, produced quantitative data in very good agreement with measured concentration profiles; however, its results are system specific. We therefore provide here a different and somewhat cruder analysis, to propose simple but general criteria for estimating the influence exerted by the reinforcement on microsegregation in the matrix.

It is well known that in the solid-state homogenization of a cored alloy, at longer times, the degree of homogenization is well described by the first term of a series solution, of wavelength equal to the dendrite arm spacing λ.[19,32] For homogenization at a constant temperature, the time required for reduction of concentration differences to a fraction f of their initial values is thus roughly given by

$$t_h \approx -\lambda^2 (\pi^2 D_s)^{-1} \ln (f) \qquad [26]$$

where λ is the wavelength of the concentration distribution and D_s the solid-state diffusion coefficient at the homogenization temperature.

We now consider the composite matrix solidified slowly: we know that λ is at most on the order of Λ, the interstice width, and D_s is at least equal to the solid-state diffusion coefficient at the eutectic temperature, D_{eut}. Therefore, if the total solidification time of the composite is t_{fc}, we know that because the rate of diffusion is most sluggish at the eutectic temperature, concentration differences in the alloy will be reduced to a fraction f of their maximum values (given by the Scheil equation) if

$$t_f \geq -\Lambda^2 (\pi^2 D_{eut})^{-1} \ln (f) \qquad [27]$$

Taking $f = 0.01$ as a criterion for essentially no coring

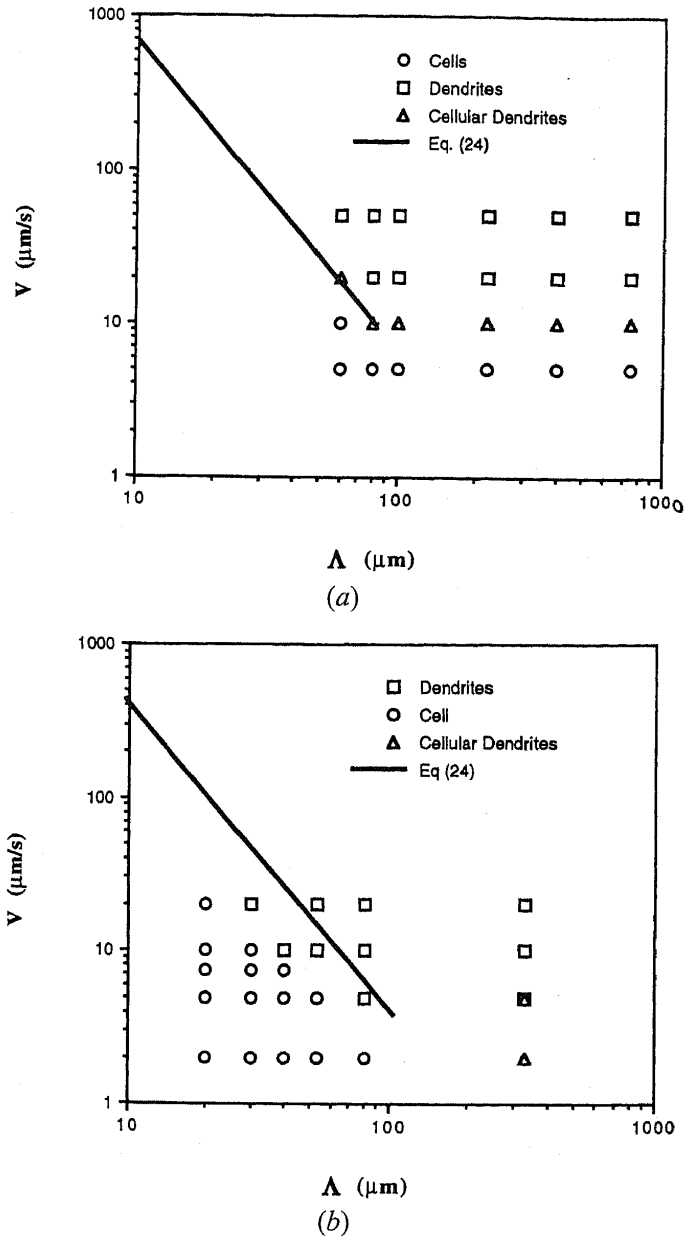

Fig. 4—Microstructural transitions for steady-state directional solidification with $G = 4$ K mm^{-1}: (*a*) for succinonitrile-0.3 wt pct acetone in cylindrical channels and (*b*) for succinonitrile-0.5 wt pct acetone in rectangular channels. The straight line corresponds to the predicted dendrite to cell transition (Eq. [24]) plotted in its domain of validity (*i.e.*, for V above the cell to dendrite transition in the unreinforced alloy).

in the matrix, we then expect an essentially featureless matrix in the composite if

$$t_f \geq 0.5\ \Lambda^2 (D_{eut})^{-1} \qquad [28]$$

For Al-Cu alloys, $D_{eut} = 1.4 \times 10^{-13}$ m^2 s^{-1}, so that a featureless matrix is predicted for $t_f \geq 3\ 10^{12}\ \Lambda^2$ (in SI units). This is relatively close to (and, as expected, a bit more conservative than) the finite-difference computer analysis of Reference 27, which predicted a featureless matrix in this system when $t_f \geq 1.3\ 10^{12}\ \Lambda^2$.

In summary, inserting Eq. [2] into Eq. [28], the composite matrix will be free of microsegregation if

$$H\Lambda^2 \leq 2D_{eut} [(1 - V_f) L_f + c_e \Delta T] \qquad [29]$$

Conversely, if solidification is sufficiently rapid, solid-state diffusion will not erase concentration gradients in the

matrix faster in the composite compared to the unreinforced alloy. An upper bound for the extent of solid-state diffusion in dendritic solidification was derived in References 19,33 showing that in solidification of a binary alloy, if $\alpha = 4D_s t_{fc} \lambda^{-2}$, where λ is the final dendrite arm spacing, is less than about 0.1, solid-state diffusion exerts little influence on microsegregation. Since the reinforcement will only exert an influence on microsegregation in the matrix if Λ is smaller than the dendrite arm spacing in the unreinforced alloy, we expect essentially no effect of the reinforcement on matrix alloy microsegregation if

$$t_f \leq \Lambda^2 / 40 D_{s1/2} \qquad [30]$$

where $D_{1/2}$ is an average value of D_s over the solidification range of the composite. Taking $D_{s1/2}$ to be the diffusion coefficient midway through the solidification range of Al-4.5 wt pct Cu (at 600 °C), this criterion predicts essentially no reduction in microsegregation by solid-state diffusion in this alloy if $t_f \leq 6\ 10^{10}\ \Lambda^2$. This also compares well with finite-difference computer simulations for Al-4.5 wt pct Cu, which yielded $t_f \leq 10^{11}\ \Lambda^2$ for no effect of solid-state diffusion on matrix microsegregation. In conclusion, we expect no anomalously reduced alloy microsegregation in the composite by enhanced solid-state diffusion if

$$H\Lambda^2 \leq 40 D_{s1/2} [(1 - V_f) L_f + c_c \Delta T] \qquad [31]$$

A second mechanism exists for the reduction of microsegregation in metal matrix composites, namely, increased undercooling of the tip, under solidification conditions where cells form instead of dendrites; as shown in Section V, these form roughly when Eq. [24] is satisfied.

Neglecting now solid-state diffusion, we can use correlations from the analyses of Karma and Pelcé (for a cell growing in a planar interstice of width Λ at low Peclet number) or of Lu and Hunt (for a cylindrical cell growing at steady state), summarized in a previous review of steady-state directional solidification of binary composite matrices,[3] to predict the dimensionless cell tip undercooling defined by

$$T_t = T_0 + \Delta \frac{mC_0 (1 - k)}{k} \qquad [32]$$

where T_t is the tip temperature and T_0 the liquidus temperature at liquid composition C_0. Using the correlation of Lu and Hunt for the growth conditions of present interest, Δ is given by

$$\Delta = \frac{k}{2} + \frac{\sqrt{\frac{2k(2 - k)\Gamma V}{(1 - k) \mid m \mid C_0 D}} + \left(1 - \frac{k}{2}\right)}{\left(1 - \frac{k}{2}\right)^{2/3} (\pi N)^{4/3}} \qquad [33]$$

where N is defined as

$$N = \frac{\Lambda}{2\pi} \sqrt{\frac{\frac{-mVC_0 (1 - k)}{kD} - G}{\Gamma}} \qquad [34]$$

and simplifies to

$$N = \frac{\Lambda}{2\pi} \sqrt{\frac{-mVC_0 (1 - k)}{kD\Gamma}} \qquad [35]$$

for the solidification conditions considered here. The first term in the numerator of Eq. [33] can often be neglected. This is in particular the case for binary aluminum alloys with $V \leq 1$ cm s^{-1}. Equation [33] is then simplified significantly to become

$$\Delta = \frac{k}{2} + \left(1 - \frac{k}{2}\right)^{\frac{1}{3}} (\pi N)^{-\frac{4}{3}} \qquad [36]$$

Counting $\Delta \geq 0.1$ (for $k < 0.2$) to correspond to a significant increase in undercooling due to geometrical constraint, we expect a reduction in microsegregation due to this effect when

$$V\Lambda^2 \leq \frac{-4kD\Gamma \left(1 - \frac{k}{2}\right)^{\frac{1}{6}}}{mC_0 (1 - k) \left(0.1 - \frac{k}{2}\right)^{\frac{1}{2}}} \qquad [37]$$

As for the transition to cellular growth treated in Section V, V must be estimated. This increase in undercooling will essentially eliminate microsegregation (thus forcing the matrix to solidify close to the plane-front configuration due to capillary effects) when Δ approaches 1; however, it is apparent from Figure 3 of Reference 3 that the solidification morphology may become quasiplanar before then. Therefore, taking $\Delta = 1$ in Eq. [36], it can only be concluded that

$$V\Lambda^2 \leq \frac{-4kD\Gamma \left(1 - \frac{k}{2}\right)^{\frac{1}{6}}}{mC_0 (1 - k) \left(1 - \frac{k}{2}\right)^{\frac{1}{2}}} \qquad [38]$$

is a conservative estimation of the onset of essentially full suppression of microsegregation by capillary effects in the matrix (we note that curvature in quasiplane front solidification with $\theta \neq \pi/2$ will cause some microsegregation in the matrix).

VII. DISCUSSION

A. *Microstructure Transition Maps for Al-4.5 Wt Pct Cu*

To recapitulate, theoretical analysis predicts that a reinforced hypoeutectic binary alloy, solidified under conditions where the unreinforced matrix forms dendrites, can (1) become nondendritic in a composite, due to dendrite arm coalescence or by transition to cellular growth, and (2) show significant reductions, or even elimination, of microsegregation in the as-cast condition.

We derive criteria for these microstructural transitions, expressed in terms of H, Λ, and system parameters, save for criteria predicting the onset and consequences of cellular growth in the composite, which necessitate knowledge of the growth rate V or at least the grain size d of an equiaxed matrix alloy. Since we have assumed no enhanced nucleation of the matrix onto the reinforcing phase, d can be estimated to be the same as in an unreinforced casting

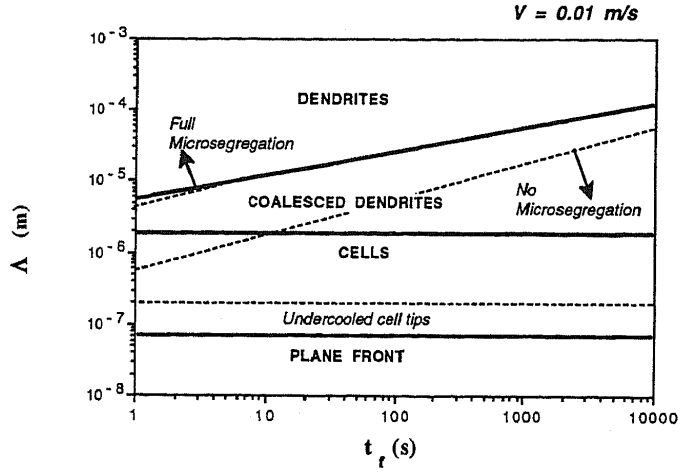

(a)

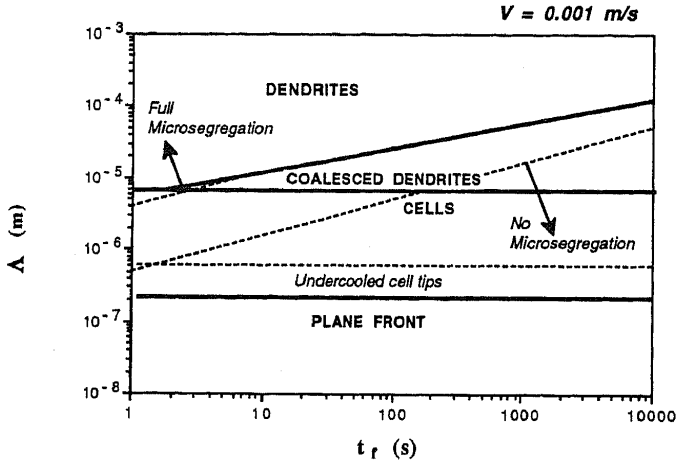

(b)

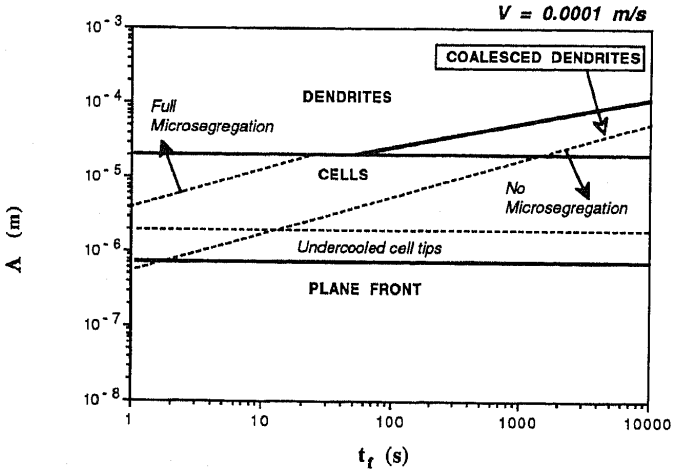

(c)

Fig. 5—(*a*) through (*c*) Microstructure maps for Al-4.5 wt pct Cu solidified at constant rate of enthalpy loss, plotted as a function of the corresponding solidification time t_f (Eq. [2]), and the width of the interstice between reinforcing elements, Λ. Continuous lines denote microstructural transitions, corresponding from top to bottom to Eqs. [22], [24], and [38], this last criterion being very conservative and probably path dependent. Dotted lines denote transitions in microsegregation in the alloy, corresponding from top to bottom to Eqs. [31], [29], and [37].

of the same alloy cooled analogously. However, this is a rough first approximation, because (1) differences between the thermophysical properties of the composite and those of the unreinforced alloy may cause changes in nucleation rate at constant H; (2) impingement of the growing solid on the reinforcement may provide time for formation of more nuclei in the composite, causing a reduction in grain size (an effect analogous to that explored by Pezzee and Dunand for recrystallization in composites[34]); and (3) if there is convection in an analogous unreinforced casting, grain size increases may result in the composite because such convection will be suppressed by the stationary reinforcement assumed here.[2]

Predicted microstructural transitions are plotted in Figure 5 for Al-4.5 wt pct Cu as a function of solidification time t_f and Λ for three plausible values of the growth velocity V (thermophysical data are given in the Appendix). In these microstructural maps, thick full lines denote changes in growth form, while the dotted lines indicate changes in the level of solute segregation within the alloy.

At the highest cooling rates and with large reinforcement diameters, the matrix of the composite remains dendritic. This is as expected, as the finest dendrites have ample room to grow with minimal perturbation from large reinforcing elements. In this growth regime, which furthermore is seen not to cause greatly reduced microsegregation in the matrix, the alloy microstructure features visible secondary dendrite arms together with pools of eutectic phase, both along the fiber/matrix interface and between dendrite arms.

As the reinforcing element size decreases and as the solidification time increases, dendrites form initially in the solidification process but coarsen and coalesce to erase all dendrite arms. In the later stages of the solidification process, solidification is thus nondendritic. The matrix second phase is then concentrated along the matrix/reinforcement interface, and depending on how early in the solidification process coalescence erased dendrite arms, coring patterns run parallel to the fiber/matrix interface. It is also seen that within this growth regime, at yet longer solidification times, solid-state diffusion reduces microsegregation significantly, to the point where an as-cast fully homogenized composite matrix is formed below the dotted line corresponding to Eq. [29].

Below the top horizontal V-dependent line corresponding to Eq. [24], cells are predicted to form instead of dendrites. Here, the alloy solid/liquid interface is expected to run parallel to the matrix/reinforcement interface, as in a coalesced dendritic microstructure but from the very onset of solidification. It is interesting to note that for this alloy at least, only very fine reinforcements, near or below a micrometer in diameter, are expected to cause significant enhancements in cell tip undercooling and *a fortiori* a transition to pseudo-plane front solidification. Such composites have been produced by solidification processing;[35] however, very little characterization of their cast microstructure has been published to date. Since most of the field corresponding to undercooled cell tip formation lies significantly below the line for full matrix homogenization by solid-state diffusion, these transitions will not be reflected in the fully solidified microstructure unless V is below 100 μm/s and t_f below 10 seconds.

On the other hand, at low V and low t_f, the dendrite to cell transition should be visible in some as-cast composites: in these regions of the map, below the dendrite to cell transition line, significant microsegregation is predicted and dendrite arms do not have time to coalesce. In this region

of the map, therefore, the dendrite to cell transition is predicted to produce visible departures of the fully solidified composite matrix structure, concentrating all the eutectic and higher-concentration primary phase near the matrix/reinforcement interface. Although composites have been solidified with t_f near a second, V must have been high enough for this transition not to have taken place since no observation of this transition has, to the best of the authors' knowledge, been published to date for reinforced metals.

B. *Comparison of Theory with Experiment*

We compare theory with experiment using two studies of composite solification, one on Al-4.5 wt pct reinforced with about 50 vol pct long alumina fibers 20 μm in diameter[26] and the other on Al-6 wt pct Cu reinforced with 30 vol pct long alumina fibers 3 μm in diameter.[36] In both studies, no evidence of cell formation was found; in the latter study, it was furthermore shown using interrupted solidification experiments that under the slowest cooling conditions, solidification was initially dendritic. Therefore, we assume that solidification velocities were too high for cell formation and compare theory with experiment in terms only of the microstructural transitions predicted for initially dendritic solidification. For simplicity, horizontal lines corresponding to Eqs. [24], [37], and [38] are therefore not plotted on the maps.

Microstructures from the former study are shown in Figure 6. It is seen that the reinforcement is quite homogeneously distributed; using the equations of Section III, we find $\Lambda = 20$ μm in these composites. Knowing the solidification times for these four samples, we plot corresponding experimental data points on the microstructural transitions map for this alloy (Figure 7). It is seen that observed microstructural transitions are in complete agreement with theory. For $t_f = 1.3$ seconds, a dendritic microstructure, with visible secondary dendrite arms, is indeed observed. For $t_f = 18$ seconds, dendrite arms have disappeared from transverse cross sections but are still visible along the fiber direction, indicating that, indeed, this sample is near the threshold for dendrite arm coalescence. For $t_f = 192$ seconds only a few occasional pools of eutectic are found joining fibers, and microsegregation is still present, since significant quantities of nonequilibrium eutectic are still found near the fibers, and electron microprobe measurements of the minimum copper concentration in the matrix (Figure 8) yield about 1.5 wt pct Cu,[26] a value only a little above $kC_0 = 0.8$ wt pct Cu. For $t_f = 750$ seconds, no dendrite arms are visible and hardly any eutectic is found near the fibers, indicating that there is very little microsegregation in the matrix. Measurement of the minimum copper concentration in the matrix (Figure 8) confirms this, since the minimum copper concentration is near 3 wt pct Cu: this sample is, indeed, predicted to have only little residual microsegregation (Figure 7). For $t_f = 1000$ seconds, the minimum copper concentration measured by electron microproble analysis in the matrix is 4 pct (Figure 8): this is also in agreement with theory, which predicts that for this solidification time, the matrix should be essentially free of microsegregation.

Experimental data points from the study of Li *et al.*[36] are compared with theory in Figure 9. In these composites, because of the lower fiber volume fraction, the fiber distribution is less homogeneous; however, we nonetheless use a value for Λ computed using the formulas of Section III, $\Lambda = 7$ μm. It is seen that for $t_f = 1$ seconds, a dendritic microstructure is predicted for this composite, in agreement with theory. For all other samples, coalesced dendrites are predicted, and the transition from dendrites to coalesced dendrites is said, by the authors, to take place near $t_f = 10$ seconds, as predicted Figure 9. For $t_f = 520$ seconds the microstructure shows a significant reduction in the volume fraction eutectic compared to the sample with $t_f = 1$ seconds, and microprobe measurements of the minimum copper concentration in the largest interstices of the composites yield a minimum copper concentration of 4.6 wt pct Cu, quite near the solidus composition at the eutectic temperature, of 5.65 wt pct Cu. Microsegregation is, in this sample, nearly eliminated, again in agreement with theory. Agreement between theory and experiment is, thus, again very satisfactory.

C. *Limitations of Theory*

The main word of caution that must be applied before equations and graphs derived here are applied in practice relates to two of the assumptions made in Section B concerning the reinforcement: that the reinforcement be homogeneously distributed and that it be immobile. If the reinforcement is mobile, as is typically the case in particulate-reinforced alloys of V_f below about 30 vol pct, at high θ, particle pushing renders the reinforcement distribution inhomogeneous and variable in time. The dendrite arm spacing of such alloys can increase far above the reinforcing particle diameter as H decreases, at a rate that is relatively little affected by the presence of the reinforcement (*e.g.*, References 37 through 42). In these composites, matrix solidification is less affected by the reinforcement, and the matrix microstructure is expected to be closer to that of the unreinforced matrix.

The second word of caution is related to the assumption of reinforcement homogeneity. Although many high-volume fraction metal matrix composites feature relatively homogeneous microstructures, there is always some inhomogeneity in the packing of the reinforcement, with the implication that there is always a range of distribution of Λ around the average value derived previously. The range of variation of Λ must therefore be considered in applying the microstructural rules derived here. This is especially important in some composites which feature an essentially bimodal interstice width distribution. These are found with parallel continuous fiber composites of low V_f, in which fibers can be strongly clustered into the original fiber tows, either in the fiber preform before it is combined with the matrix (*e.g.*, when fiber tows are woven into three-dimensional braided preforms[43]) or due to capillary effects during infiltration when the tows are loosely packed (*e.g.*, References [44 and 45]). An extreme case is, of course, also that of selectively reinforced composite components. In such composites, simultaneous optimization of microstructure in both the high-V_f regions and in wide reinforcement-free regions places strong restrictions on the exploitability of the novel microstructures that can be generated in the matrix of the composite: for example, microsegregation reduction by prolonged hold in the mushy zone of the alloy would have disastrous consequences in the unreinforced portions of these components.

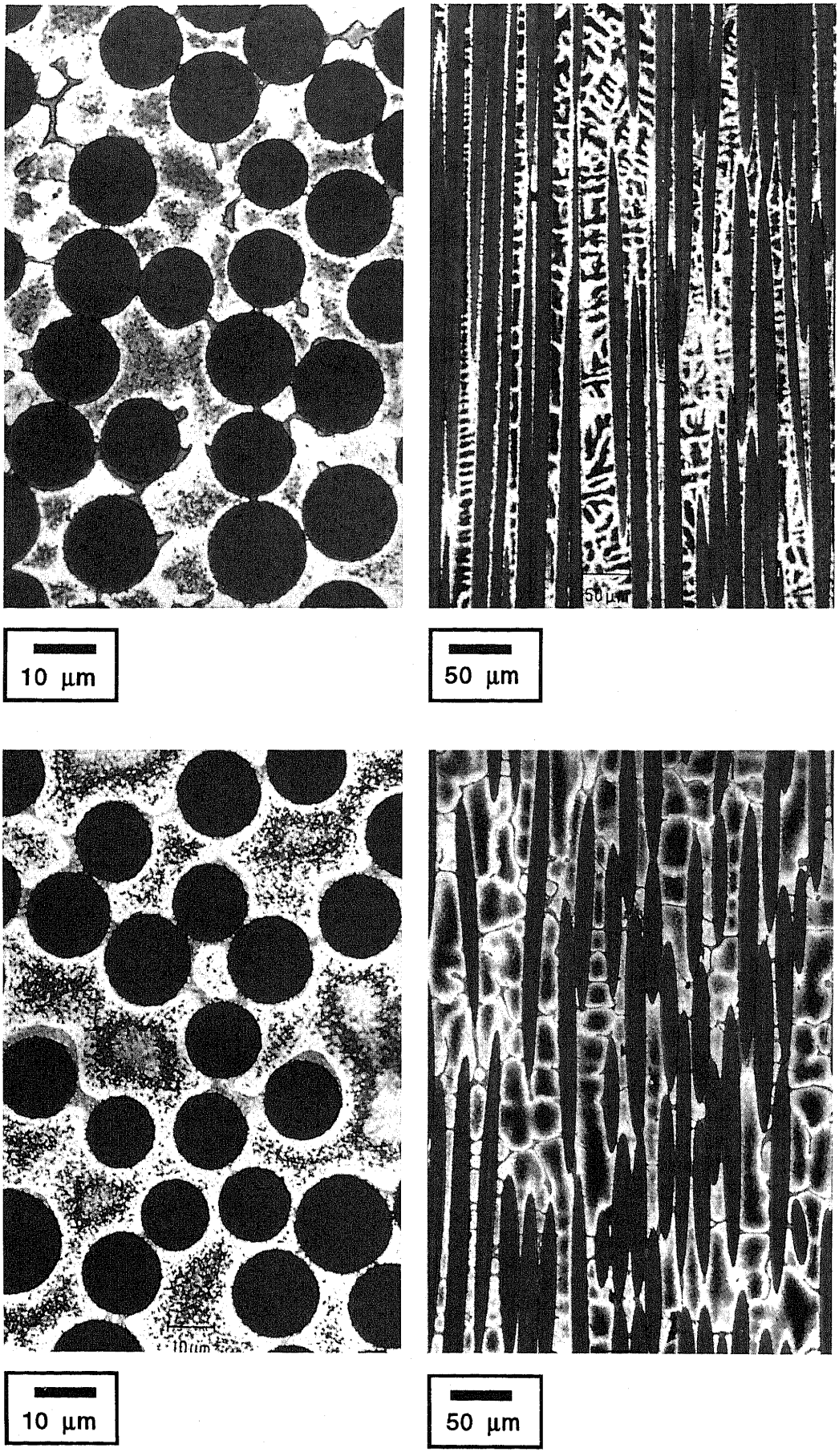

Fig. 6—Transverse and longitudinal microstructures of Al-4.5 wt pct Cu reinforced with 50 vol pct continuous alumina fibers, with (*a*) t_f = 1.3 s, (*b*) t_f = 18 s, (*c*) t_f = 192 s, and (*d*) t_f = 520 s.[26]

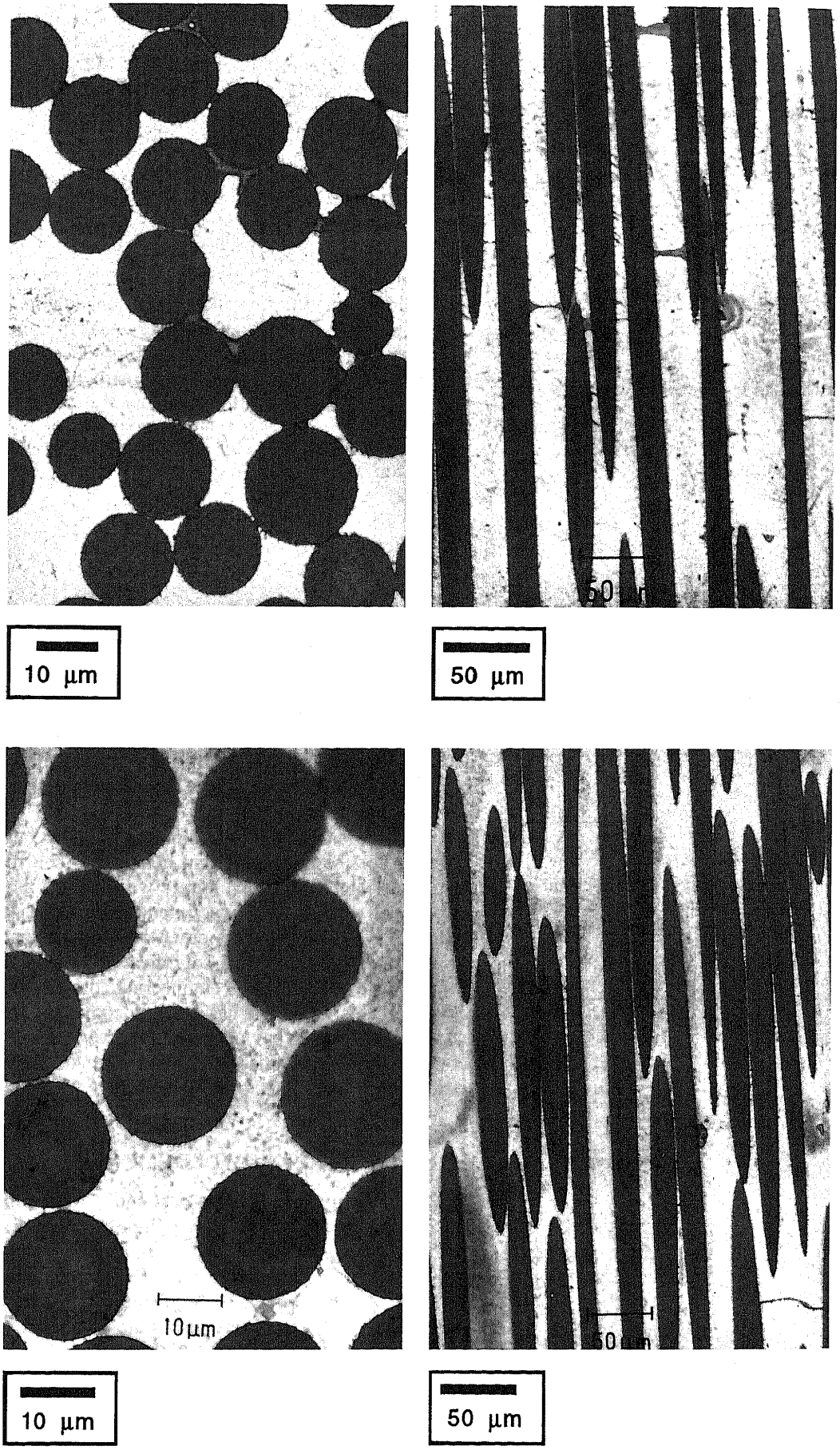

Fig. 6—Transverse and longitudinal microstructures of Al-4.5 wt pct Cu reinforced with 50 vol pct continuous alumina fibers, with (*a*) t_f = 1.3 s, (*b*) t_f = 18 s, (*c*) t_f = 192 s, and (*d*) t_f = 520 s.[26]

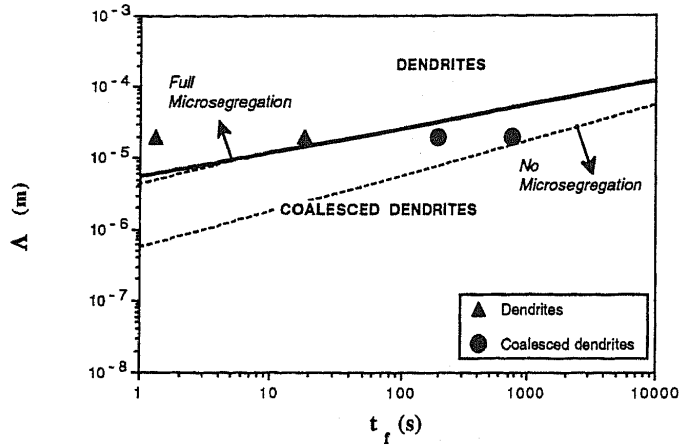

Fig. 7—Comparison of dendrite microstructural transitions in samples of Fig. 6 with theory.

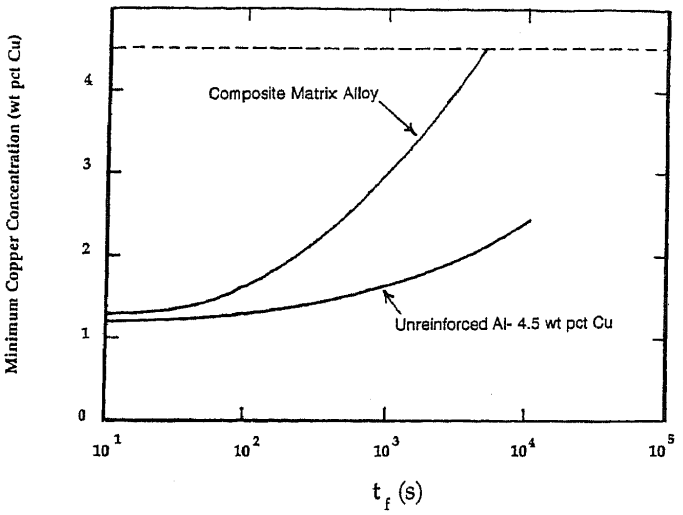

Fig. 8—Minimum copper concentration in Al-4.5 wt pct Cu, unreinforced and reinforced with 50 vol pct alumina fibers 20 μm in diameter as a function of solidification time t_f, measured using electron microprobe analysis.[26]

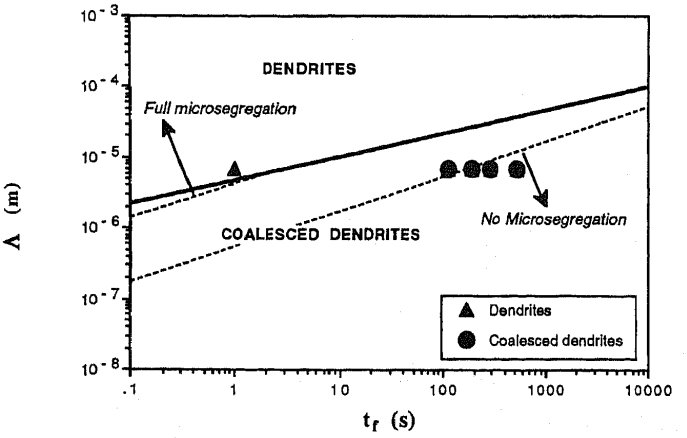

Fig. 9—Comparison of theory with experimental data from Ref. 36 for Al-6 wt pct Cu reinforced with 30 vol pct alumina fibers.

These caveats having been mentioned, within the approximations made in derivations and experimental error, most predicted microstructural transitions show good agreement with experiment, both for transitions from dendrites to coalesced dendrites and for microsegregation reduction in Al-Cu alloys and for the transition from dendrites to cells in succinonitrile-acetone. More experimental work remains for the present analysis to be fully confirmed, and there is certainly ample room for refinements and modifications of the theory; however, we believe that the equations and maps derived here provide a useful methodology for the interpretation and prediction of microstructure in cast engineering metal matrix composites.

VII. CONCLUSIONS

When a binary hypoeutectic alloy is solidified in the presence of a significant volume fraction of immobile reinforcement, which does not catalyze nucleation of the matrix alloy, and under conditions which produce dendrites in the unreinforced alloy, several microstructural transitions can be caused by the reinforcement.

1. The dendrite arms may coalesce, to evolve during solidification into a nondendritic primary phase mapping the geometry of interstices delineated by reinforcement elements.
2. Microsegregation in the matrix may be significantly reduced, or eliminated, by diffusion in the primary solid matrix phase.
3. Cells may form instead of dendrites, these cells featuring significant undercoolings or a nearly plane front configuration when reinforcing elements are very fine.

Quantitative criteria for all these transitions are derived, based on previous work on composite solidification, observations from directional solidification experiments, and current solidification theory. These show good agreement with experimental data.

We contribute in particular an approximate but simple criterion for the transition from dendrite to cell formation in a fixed interstice, which agrees with current theory and directional solidification experiments within a factor 2 in the growth velocity V. This criterion indicates that at low growth velocities and short solidification times, cells may form instead of dendrites in engineering composite castings. Although this transition has been documented for succinonitrile-acetone, it has not been observed in engineering composite castings; this would form the subject of interesting future experimental investigations.

ACKNOWLEDGMENTS

We gratefully acknowledge past and current support for our work on the solidification of composites from the Office of Naval Research, under Dr. Steven Fishman, and the National Science Foundation, under Dr. Bruce MacDonald. Stimulating discussions with Professor Alain Karma, Northeastern University, are also gratefully acknowledged.

APPENDIX
Thermophysical data

For Al-Cu alloys, the following data are used:
$D = 3.5 \times 10^{-9}$ m^2/s;[46]
$\Gamma = 2.41 \times 10^{-7}$ Km;[47]
$D_S = 0.29 \exp(-15{,}700/T) \times 10^{-4}$ m^2 s^{-1};[48]
$L_f = 9.5 \times 10^8$ J m^{-3};[32]

$c_m = 2.58 \times 10^6$ J m^{-3} K^{-1};[32] and
$K = 10^{-5}$ m s$^{-1/3}$ (approximation of $\lambda = 7.5 \times 10^{-6} t_f^{0.39}$ in SI units.)[19]

The phase diagram is simplified by assuming that the liquidus and the solidus are straight lines. This yields $k = 0.171$ and $m = -3.4$ K/wt pct Cu, $T_m = 660$ °C, $T_E = 548$ °C, and $C_E = 33$ wt pct Cu.

For alumina, $c_f = 4 \times 10^6$ J m^{-3} K^{-1}.[49] The heat capacity of the composite is given by $c_c = V_f c_f + (1 - V_f) c_m$.

REFERENCES

1. R. Trivedi, S.H. Han, and J.A. Sekhar: in *Solidification of Metal-Matrix Composites*, Proc. Conf., Indianapolis, IN, 1989, P.K. Rohatgi, ed., TMS-AIME, Warrendale, PA, 1989, pp. 23-37.
2. A. Mortensen and I. Jin: *Int. Mater. Rev.*, 1992, vol. 37, pp. 101-28.
3. A. Mortensen: *Mater. Sci. Eng.*, 1993, vol. A173, pp. 205-12.
4. A. Mortensen, L.J. Masur, J.A. Cornie, and M.C. Flemings: *Metall. Trans. A*, 1989, vol. 20A, pp. 2535-47.
5. A. Mortensen and V. Michaud: *Metall. Trans. A*, 1990, vol. 21A, pp. 2059-72.
6. S. Ho and A. Saigal: *Scripta Metall. Mater.*, 1994, vol. 31, pp. 351-56.
7. M.A. Khan and P.K. Rohatgi: in *Microstructure Formation during Solidification of Metal Matrix Composites*, Proc. Conf., Chicago, IL, 1992, P.K. Rohatgi, ed., TMS, Warrendale, PA, 1993, pp. 97-116.
8. M.A. Khan and P.K. Rohatgi: *Compos. Eng.*, 1993, vol. 3, pp. 995-1006.
9. L.M. Fabietti and J.A. Sekhar: in *Nature and Properties of Semi-Solid Materials*, Proc. Conf., San Diego, CA, 1991; J.A. Sekhar and J. Dantzig, eds., TMS Warrendale, PA, 1991, pp. 41-67.
10. L.M. Fabietti and J.A. Sekhar: *Metall. Trans. A*, 1992, vol. 23A, pp. 3361-68.
11. L.M. Fabietti and J.A. Sekhar: *J. Mater. Sci.*, 1994, vol. 29, pp. 473-77.
12. A. Mortensen and M.C. Flemings: *Metall. Mater. Trans. A*, 1996, vol. 27A, pp. 595–609.
13. N.F. Dean, A. Mortensen, and M.C. Flemings: in *Principles of Solidification of Cast Composites*, Proc. Conf., Chicago, IL, 1992, P.K. Rohatgi, ed., TMS, Warrendale, PA, 1993, pp. 83-96.
14. W. Wang, F. Ajersch, and J.P.A. Löfvander: *Mater. Sci. Eng.*, 1994, vol. A187, pp. 65-75.
15. A. Mortensen, M.N. Gungor, J.A. Cornie, and M.C. Flemings: *J. Met.*, 1986, vol. 38, pp. 30-35.
16. J.D. Bryant, L. Christodoulou, and J.R. Maisano: *Scripta Metall. Mater.*, 1990, vol. 24, pp. 33-38.
17. A. Luo: *Scripta Metall. Mater.*, 1994, vol. 31, pp. 1253-58.
18. R. Trivedi and W. Kurz: *Int. Mater. Rev.*, 1994, vol. 39, pp. 49-74.
19. M.C. Flemings: *Solidification Processing*, McGraw-Hill, New York, NY, 1974, pp. 328-34 and 141-46.
20. E.E. Underwood: *Quantitative Stereology*, 1st ed., Addison-Wesley Publishing Company, Reading, MA, 1970, ch. 4.
21. J.A. Sekhar and R. Trivedi: *Mater. Sci. Eng.*, 1989, vol. A114, pp. 133-46.
22. L.M. Fabietti, V. Seetharaman, and R. Trivedi: *Metall. Trans. A*, 1990, vol. 21A, pp. 1299-1310.
23. J.A. Sekhar and R. Trivedi: *Mater. Sci. Eng.*, 1991, vol. A147, pp. 9-21.
24. K.P. Young and D.H. Kirkwood: *Metall. Trans. A*, 1975, vol. 6A, pp. 197-205.
25. A. Mortensen: *Metall. Trans. A*, 1989, vol. 19A, pp. 247-53.
26. M.N. Gungor, J.A. Cornie, and M.C. Flemings: in *Cast Reinforced Metal Composites*, Proc. Conf., Chicago, IL, 1988, S.G. Fishman and A.K. Dhingra, eds., ASM INTERNATIONAL, Metals Park, OH, 1988, pp. 39-45.
27. A. Mortensen, J.A. Cornie, and M.C. Flemings: *Metall. Trans. A*, 1988, vol. 19A, pp. 709-21.
28. J.D. Hunt and S.Z. Lu: *Mater. Sci. Eng.*, 1993, vol. A173, pp. 79-83.
29. S.Z. Lu and J.D. Hunt: *J. Cryst. Growth*, 1992, vol. 123, pp. 17-34.
30. A. Karma and P. Pelcé: *Phys. Rev. A*, 1989, vol. 39, pp. 4162-69.
31. N.F. Dean, A. Mortensen, and M.C. Flemings: *Metall. Mater. Trans. A*, 1994, vol. 25A, pp. 2295-2301.
32. W. Kurz and D.J. Fisher: *Fundamentals of Solidification*, 3rd ed., Trans Tech Publications, Aedermannsdorf, Switzerland, 1989, pp. 289-92.
33. H.D. Brody and M.C. Flemings: *Trans. TMS-AIME*, 1966, vol. 236, pp. 615-24.
34. C.F. Pezzee and D.C. Dunand: *Acta Metall. Mater.*, 1994, vol. 42, pp. 1509-24.
35. A.M. Redsten, E.M. Klier, A.M. Brown, and D.C. Dunand: *Mater. Sci. Eng.*, 1995, in press.
36. Q.F. Li, D.G. McCartney, and A.M. Walker: *J. Mater. Sci.*, 1991, vol. 26, pp. 3565-74.
37. D.J. Lloyd: *Compos. Sci. Technol.*, 1989, vol. 35, pp. 159-79.
38. H. Lagacé and D.J. Lloyd: *Can. Metall. Q.*, 1989, vol. 28, pp. 145-52.
39. D. Lloyd: in *Metal Matrix Composites—Processing, Microstructure and Properties, 12th Risø Int. Symp. on Materials Science*, Proc. Conf., Risø, Denmark, 1991, N. Hansen, D. Juul-Jensen, T. Leffers, H. Lilholt, T. Lorentzen, A.S. Pedersen, O.B. Pedersen, and B. Ralph, eds., Risø National Laboratory, Roskilde, Denmark, 1991, pp. 81-99.
40. S. Gowri and F.H. Samuel: *Metall. Trans. A*, 1992, vol. 23A, pp. 3369-76.
41. A. Kolsgaard, L. Arnberg, and S. Brusethaug: *Mater. Sci. Eng.*, 1993, vol. A173, pp. 243-50.
42. P.K. Rohatgi, K. Pasciak, C.S. Narendranath, S. Ray, and A. Sachdev: *J. Mater. Sci.*, 1994, vol. 29, pp. 5357-66.
43. A.P. Majidi, J.M. Yang, and T.W. Chou: in *Interfaces in Metal Matrix Composites*, Proc. Conf., New Orleans, LA, 1986, A.K. Dhingra and S.G. Fishman, eds., TMS, Warrendale, PA, 1986, pp. 27-44.
44. Z. Xia, Y. Zhou, Z. Mao, and B. Shang: *Metall. Trans. B*, 1992, vol. 23B, pp. 295-302.
45. Z. Xia, Z. Mao, and Y. Zhou: *Z. Metallkd.*, 1991, vol. 82, pp. 766-68.
46. M.P. Watson and J.D. Hunt: *Metall. Trans. A*, 1977, vol. 8A, pp. 1793-98.
47. M. Gunduz and J.D. Hunt: *Acta Metall.*, 1985, vol. 9, pp. 1651-72.
48. J.B. Murphy: *Acta Metall.*, 1961, vol. 9, pp. 563-69.
49. L.J. Masur, A. Mortensen, J.A. Cornie, and M.C. Flemings: *Metall. Trans. A*, 1989, vol. 20A, pp. 2549-57.